NJC

Accepted Manuscript

This is an *Accepted Manuscript*, which has been through the Royal Society of Chemistry peer review process and has been accepted for publication.

Accepted Manuscripts are published online shortly after acceptance, before technical editing, formatting and proof reading. Using this free service, authors can make their results available to the community, in citable form, before we publish the edited article. We will replace this *Accepted Manuscript* with the edited and formatted *Advance Article* as soon as it is available.

You can find more information about *Accepted Manuscripts* in the Information for Authors.

Please note that technical editing may introduce minor changes to the text and/or graphics, which may alter content. The journal's standard Terms & Conditions and the Ethical guidelines still apply. In no event shall the Royal Society of Chemistry be held responsible for any errors or omissions in this *Accepted Manuscript* or any consequences arising from the use of any information it contains.

ROYAL SOCIETY OF CHEMISTRY

www.rsc.org/njc

Fluorescence Detection of Aromatic Amines and Photocatalytic Degradation of Rhodamine B under UV light irradiation by Luminescent Metal-Organic Frameworks

Fengqin Wang [a]*, Caifu Dong [a], Chengmiao Wang [a], Zongchao Yu [a], Shukun Guo [b], Zechuan Wang [a], Yongnan Zhao [b], Guodong Li [c]

[a]*College of Environmental and Chemical Engineering & Key Lab of Hollow Fiber Membrane Materials & Membrane Process, Tianjin Polytechnic University, Tianjin 300387, China*

[b]*School of Materials Science and Engineering & Tianjin Key Lab of Fiber Modification and Functional Fiber, Tianjin Polytechnic University, Tianjin 300387, China*

[c]*The State Key Laboratory of Inorganic Synthesis and Preparative Chemistry, Jilin University,130023, China*

E-mail: wangfengqin@tjpu.edu.cn Tel: (+86)-22-83955457

Abstract: Detection of trace amounts of aromatic amines is significantly important for security concerns and pollution control. Two multifunctional metal-organic frameworks (MOFs), $[ZnL\cdot H_2O]_n$ (**1**) and $[CdL\cdot H_2O]_n\cdot 2nH_2O$ (**2**) (L = 5-aminoisophthalic acid), were strategically chosen to utilize for the detection of aromatic amines pollutants. The fluorescent experiments show that the two MOFs can selectively detect aromatic amines with high sensitivity. Among the given analytes, *p*-nitroaniline, an electron-deficient analyte, significantly quenched the fluorescence intensities of **1** and **2**. In contrast, other aromatic amines enhanced the fluorescence intensities of **1** and **2** to some extents. Particularly, diphenylamine gives the most apparent enhancement effect than those of others under the same experimental conditions. Meanwhile, the photocatalytic activities of the two MOFs were also determined by UV light induced photodegradation of Rhodamine B (RhB) experiments. All the results indicate that the studied complexes are stable and good candidates for both heterogeneous photocatalyst and aromatic amines detectable materials.

Keywords: Luminescent Metal-Organic complexes; Fluorescence detection; Aromatic amines; Photocatalytic;

1. Introduction

Aromatic amines, known as notorious environmental pollutants, are often released into the environment from chemical, textile and leather industries along with wastes and from the decomposition of azo-dyes in various daily necessities. [1] The exposure to aromatic amines even at very low concentrations is suspected to result in carcinogenicity by ingestion, inhalation and skin contact. [2–4] Therefore, the detection of aromatic amines is a growing concern for both security reasons and pollution control. Up to now, various techniques have been developed for detection of aromatic amines, such as chromatographic, [5–7] electrophoretic methods [8–10] and mass spectrometric detector (GC–MS) [11–13]. Although these documented methods worked well in the aromatic amine detection, most of them suffered from drawbacks of expensive instrumentation, complicated operation and time-consuming procesure, which made them unsuitable for on-site, quick detection. [14] The development of sensitive analytical method for rapid and efficient detection of aromatic amines is therefore not only an exigent requirement in the field of public security, but also critical for environmental protection.

Fluorescence sensing has been proven to be an alternative analytical technology for detecting aromatic amines based on fluorescence quenching or enhancement effect. In this respect, metal-organic frameworks (MOFs), as a new kind of fluorescence sensing materials, have attracted enormous attention for sensing applications due to their high interfacial surface area and tunable pore structures. [15–17] Generally, MOF-based sensing materials are usually constructed with aromatic ligands because the π electron systems of the ligands endow the MOFs with photoluminescence properties and provide potential supramolecular recognition sites for hydrogen bonds, π-π stacking and electrostatic interaction between their backbones and the analytes. [18–19] Such interactions lead to effective charge or energy transfer process between the analytes and the MOFs, which concenquently triggers the fluorescence response upon interaction, such as the variation in emission intensity or wavelength shift. [20] By using MOFs as the sensing materials, up-to-date,

some documented examples have demonstrated the detection of nitroaromatic compounds through the effective interactions between the analytes and the MOF skeletons. [14, 21–25] Although it is still scarce on fluorescence sensing aromatic amines, [26–29] the construction of luminescent MOFs for rapid and efficient detection of aromatic amines is of great significance for environmental monitoring.

Besides the detection of pollutants, on the other hand, MOFs have also attracted much attention for their applications as photocatalyst in decomposing organic contaminations because of their high surface areas and high light absorption abilities. [30–33] In general, MOFs with absorption bands in the UV region exhibit photocatalytic performance for degrading organic dyes upon UV light excitation. Recently, some literatures have reported sensing applications as well as heterogeneous photodegradation of organic dyes. [30, 34] Thus, it is highly necessary to construct multifunctional MOFs with both sensing behaviors and photocatalytic properties by the assembly of aromatic ligands and functional metal centers.

In this work, we selected 5-aminoisophthalic acid, which was widely used to construct MOFs with d^{10} metal ions, [35-39] as the organic linker to synthesize two MOFs, $[ZnL\cdot H_2O]_n$ (**1**) and $[CdL\cdot H_2O]_n\cdot 2nH_2O$ (**2**) (L = 5-aminoisophthalic acid), which structures are well documented. [35, 36] However, the applications of them in the fluorescence sensing and photocatalysis have not yet been reported. Herein, the fluorescence sensing performances and the photocatalytic activities of these two MOFs are systematically studied. The results indicate that complexes **1** and **2** are promising luminescent probes for detecting aromatic amines via fluorescence enhancement or quenching effect, which can be potentially used for pollutants detection or environmental monitoring. In addition, compounds **1** and **2** also exhibit excellent photocatalytic activities for degrading organic dyes under UV light irradiation.

2. Experimental

2.1 Materials and methods

All reagents were obtained from commercial sources and used as received.

Infrared spectra were recorded on a BIO-RAD FTS3000 system by using KBr pellets in the range 4000 − 400 cm^{-1}. Elemental analyses (C, H and N) were measured on a Perkin-Elmer auto-analyzer. Thermogravimetric (TG) analysis was carried out on a Netzsch STA 409 PG/PC analyzer at a heating rate of 5 °C min^{-1} from ambient temperature to 800 °C. Powder X-ray diffraction (PXRD) data were recorded on a D/MAX-2500 automated diffractometer. The simulated PXRD patterns were derived from the single crystal data through the diffraction-crystal module of the Mercury program version 3.0. The photoluminescence spectra of the studied complexes in solid and their samples in acetonitrile or methanol were measured on an F−380 Spectrophotometer. The UV-vis adsorption spectra were recorded by using an Evolution 201 UV-Vis Spectrometer. The solid-state diffuse-reflectance spectra for powder samples were recorded on a U-4100 Spectrophotometer spectrometer equipped with an integrating sphere by using $BaSO_4$ as a white standard.

2.2 Synthesis of $[ZnL\cdot H_2O]_n$ (1) and $[CdL\cdot H_2O]_n\cdot 2nH_2O$ (2)

Homogenized mixtures of L (18.1 mg, 0.1 mmol), $Zn(NO_3)_2\cdot 6H_2O$ (29.7 mg, 0.1 mmol), DMF (4 mL) and H_2O (4 mL) were sealed in a 25 mL stainless steel vessel and heated at 85 °C for 3 days under autogenous pressure, and then cooled to room temperature. Colorless block crystals of **1** were obtained by filtration. Elemental analysis (%) calcd for $C_8H_7NO_5Zn$: C, 36.57; H, 2.67; N, 5.33. Found: C, 36.23; H, 2.49; N, 5.63. IR spectra (KBr pellet cm^{-1}): 3442 br, 1622 vs, 1566 vs, 1478 w, 1414 m, 1367 vs, 1157 m, 966 w, 737 m. Complex **2** was obtained by a procedure similar to that for **1** but only changing the $Zn(NO_3)_2\cdot 6H_2O$ with $CdCl_2\cdot 2.5H_2O$. Colorless block crystals were obtained by filtration. Elemental analysis (%) calcd for $C_8H_{11}NO_7Cd$: C, 27.78; H, 3.18; N, 4.05. Found: C, 28.05; H, 3.51; N, 4.16. IR spectra (KBr pellet cm^{-1}): 3478 br, 1614 vs, 1566 vs, 1474 w, 1373 vs, 1098 w, 1018 w, 808 w, 767 m.

2.3 Fluorescence titrations in dispersed medium

The fluorescence spectra of compounds **1** and **2** were measured by dispersing grounded sample (3 mg) in acetonitrile (3 mL) or methanol (3 mL), respectively, which were treated by ultrasonication for 1.5 h. All titrations were carried out by gradually adding analytes in an incremental fashion. The corresponding fluorescence

emission spectra were recorded at 298 K. Each titration was repeated several times to get concordant values. For all measurements, the suspensions of **1** and **2** were excited at λ_{ex} = 310 nm and the corresponding emission wavelengths were monitored from 320 to 600 nm. The fluorescence efficiency was calculated by using the formula $[(F_0\text{-}F)/F_0] \times 100\%$ (F_0 is the initial fluorescence intensity).

2.4 Photocatalytic experiments

Photocatalytic experiments in aqueous solutions were performed in a 150 mL quartz beaker. A 300 W high-pressure mercury lamp was used as the UV light source. An aqueous solution of RhB (80 mL) with a concentration of 10^{-5} mol L^{-1} was mixed with the catalysts (20 mg) and illuminated. Before turning on the lamp, the suspension containing RhB and the photocatalyst was magnetically stirred in the dark for 40min until an adsorption-desorption equilibrium was established. At given irradiation intervals, a series of aqueous solutions of a certain volume were collected and separated by centrifugation to remove suspended catalyst particles and then subjected to UV/Vis spectroscopic measurements.

2.5 X-ray crystallography

Single crystal X−ray diffraction measurement for **1** and **2** were carried out on computer-controlled RIGAKU diffractometer equipped with graphite-monochromatized Mo-Kα radiation with a wavelength of 0.71073Å by using the ω-scan technique. The structures were solved by direct methods and refined by full-matrix least squares on F^2 using the SHELXS 97 and SHELXL 97 programs. [40, 41] Semiempirical absorption corrections were applied using the SADABS program. [42] All non-hydrogen atoms were refined anisotropically. The hydrogen atoms were generated geometrically and treated by a mixture of independent or constrained refinement. The crystallographic data for **1** and **2** are listed in Table S1, selected bond lengths (Å) and angles (°) are listed in Table S2. The hydrogen bonds data are listed in Table S3.

3. Results and discussion

3.1 Structure description of 1

The single crystal X-ray diffraction structure determinations show that both compounds **1** and **2** have 2D layer structures, which are the same as those in the literatures. So, herein, we only describe the detailed structure of **1** as an example. In the asymmetric unit of **1**, there is only one crystallographically independent zinc ion. The coordination environment is shown in Fig. 1. The zinc ion is four-coordinated with two oxygen atoms and one nitrogen atom from three different L ligands, one oxygen atom from one coordinated water molecule and displays a distorted tetrahedral geometry. The Zn−O distances are in the range of 1.9570(16) − 1.9756 (15) Å. The Zn−N distance is 2.0363(18) Å.

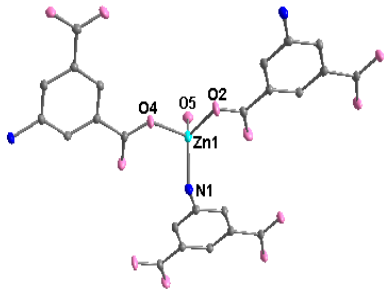

Fig. 1 The coordination environment of the Zn (II) ion in **1** with 30% probability thermal ellipsoids.

In the structure of compound **1**, each L ligand adopts tri-monodentate mode with its two carboxylate groups and one amino group coordinating to three different zinc ions. Each zinc ion is linked by three L ligands to form an infinite 2D layer structure containing a 22-membered macrocycle (Fig. 2). It is very interesting to see that, in the same layer of **1**, all of the coordinated water molecules are oriented toward the same direction. Furthermore, all of these layers, where the coordinated water molecules are oriented in opposite directions, are linked together in pairs through strong hydrogen bonds into a three-dimensional supramolecular network.

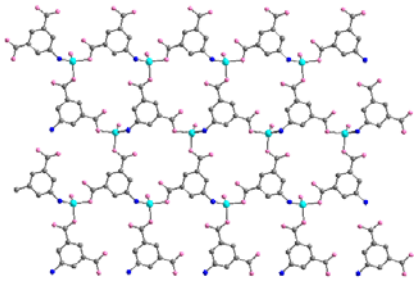

Fig. 2 The 2D layer framework of **1**

The thermal stabilities of **1** and **2** were studied by thermogravimetric analysis (TGA). The thermal decomposition process of **1** occurred in two steps (Fig. S1). The first weight loss of 7.09% between 180 and 328 °C corresponded to the release of one water molecule (calcd: 6.86%). A plateau was observed from 328 to 446°C, indicating no further weight loss. When the temperature was above 446°C, the compound started to decompose rapidly. The residue ZnO was obtained in 30.45% (calcd: 30.85%). Powder X-ray diffraction analysis was further conducted to confirm the phase purity of **1**, which was shown in Fig. S2. For **2**, the thermal decomposition process can be described in three steps (Fig. S3). The first weight loss of 9.89% between 100 and 143 °C corresponded to the release of two free water molecules (calcd: 10.41%). The second step lost a coordinated water molecule with the mass loss of 4.53% between 143 and 310°C (calcd: 5.21%). The third step mass loss began at 426°C and ended at 616°C with the product CdO formed in 37.91% (calcd: 37.15%). The PXRD pattern of the as-synthesized sample of **2** is also very close to the simulated pattern from single crystal structure (Fig. S4). This also demonstrates the phase purity of the as-synthesized sample of **2.**

3.2 The Photophysical Properties

The solid-state fluorescence spectra of **1** and **2** were recorded at room temperature. As shown in Fig. S5 and S6, the main emission band of **1** located at 415 nm (λ_{ex} = 310 nm) and that of **2** centered at 425 nm (λ_{ex} = 310 nm). For the free ligand L, the characteristic photoluminescence emission maxima located at 467 nm upon excitation at 290 nm. In comparison, the emission blue shifted by 52 nm for **1** and 42 nm for **2**, respectively. The blue-shifts of the emission peaks are probably due to substantial electronic coupling between the neighbor ligands through the d^{10} (Zn^{2+} or Cd^{2+}) metal ions. [18] We also examined the luminescence properties of **1** and **2** in common organic solvents. The emission wavelength of 415 nm for **1** in acetonitrile is the same with that of solid state sample (Fig. S7). The emission wavelength of **2** in methanol slightly shifts from 425 nm to 431 nm in comparison with that of solid sample (Fig. S8). The strong emissions of **1** and **2** in the solid state or in organic suspensions indicate their potential applications in liquid phase fluorescence

detection. Also, the diffuse reflectance spectra (DRS) obviously reveal that both **1** and **2** exhibit photoresponses in the UV region (Fig. S9 and S10). Calculations based on the Tauc equation give the band gaps (Eg) of 2.82 eV for **1** and 3.41 eV for **2**, respectively (Fig. 3a and 3b).

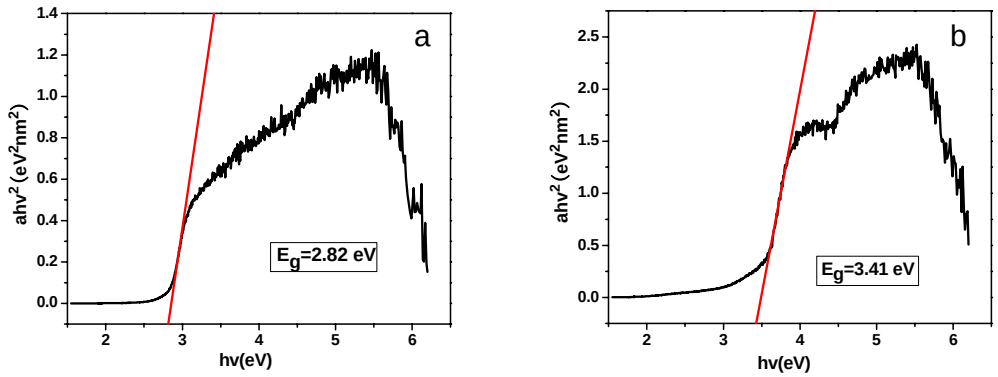

Fig. 3 Kubelka−Munk-transformed diffuse reflectance spectra of **1** (a) and **2** (b).

3.3 Detection of aromatic amines

Based on the fluorescence properties of **1** and **2**, fluorescence detection experiments were carried out with the acetonitrile suspension of **1** and the methanol suspension of **2** by gradually adding the aromatic amines. The addition of aromatic amines, such as aniline, *p*-toluidine, diphenylamine and *p*-nitroaniline, promoted the significant fluorescence quenching or enhancement in the fluorescence intensities of the two MOFs. The percentage of fluorescence quenching or enhancement for different analytes is given in Fig. 4 and Fig. 5. For the selected analytes, **1** and **2** show similar sensing behaviors. Among the given analytes, *p*-nitroaniline significantly quenched the fluorescence emissions of **1** and **2**. When the addition amount of *p*-nitroaniline was only 0.2 μmol, the fluorescence intensity of **1** at 415 nm declined by 88.92%, accompanied by a small red-shift to 430 nm (Fig. 6a). For **2**, the fluorescence intensity at 431 nm was quenched by 51.60%, accompanied by a small red-shift to 447 nm (Fig. 6b). In contrast, other aromatic amines enhanced the fluorescence intensities of **1** or **2** to various extents. Of particular interest is that compound **1** exhibits a new emission at 366 nm in addition to the original peak at 415 nm. As well, compound **2** give a new emission at 368 nm in addition to the original peak at 431 nm. Furthermore, the emission intensities enhanced drastically

with the addition of aromatic amines into the solution. Among them, diphenylamine gives the most significant enhancement under the same experimental conditions. For **1**, the fluorescence intensity at 366 nm increased greatly even at a very low concentration. The emission considerably intensified by 618.42% with the addition of only 0.2 μmol diphenylamine, along with a small red- shift of the emission wavelength. However, the original emission peak at 415 nm was slightly enhanced by 47.01% (Fig. 7a). Compared with **1**, the fluorescence intensity of **2** at 368 nm increased more drastically and reached above 2738% even by a very low dosing of only 0.03 μmol diphenylamine in the solution. Similarly, the original emission peak of **2** at 431 nm increased only by 147.8% (Fig. 7b). For *p*-toluidine and aniline, **1** and **2** also exhibit similar performances with diphenylamine except for lower enhancement degrees (Fig. S11 − S14). For **1**, the order of enhancing efficiency for the selected analytes is diphenylamine > aniline > *p*-toluidine. For **2**, however, the sequence is diphenylamine > *p*-toluidine > aniline.

In order to better assess the selectivity for sensing aromatic amines, triethylamine was selected as the probe to investigate the influence of aliphatic amine on the fluorescence of **1** and **2**. As shown in Fig. S15 and S16, no obvious change occurred in the emission intensities of the two MOFs by adding triethylamine into the acetonitrile suspension of **1** or methanol suspensions of **2**. These results demonstrate that **1** and **2** are both selectively sensitive to aromatic amines. And also, the sensitivity is prior to the literature reported complex: $[Tb(1,3,5\text{-btc})(H_2O)_6]_n$.(btc = benzene-1,3,5-tricarboxylate). [26] Such selective fluorescence variation behaviors make them potential for highly selective detection of aromatic amines.

For the two MOFs, the selective luminescence sensing of aromatic amines may be attributed to the photoinduced electron transfer between the MOFs and the analytes adsorbed on the surfaces of the MOFs. Generally, the electron transfer from the electron-donating MOFs to the highly electron-withdrawing analytes will result in the detectable luminescence quenching effect. [43, 44] The fact that *p*-nitroaniline exhibits the significant quenching effect may be attributed to the excited state electrons transfered from the frameworks of the two MOFs to analyte molecules. In

contrast, if the excited electrons transfer from the analytes to MOFs, a fluorescence enhancement effect occurs. Thus, for other aromatic amines, the observed enhancement in emission intensities and red-shifts in the emission wavelengths demonstrate that the electrons possibly transfer from the given analytes to the MOFs along with the formation of strong exciplex between them. Comparing to these electron-rich aromatic amines, diphenylamine, which has two benzene rings, can form stronger interactions with the MOFs. Thus, the strong interactions between them lead to the more effective electrons transer between them. For aliphatic amines, no obvious enhancement or quenching effects occurring may be due to the weak interactions between the aliphatic amines and **1** or **2**. And also the reduction potentials of the two MOFs were close to that of triethylamine, lacking the driving force for any photoinduced electron transfer. [45] Hence, the luminescence properties of the MOFs materials were unaffected by triethylamine. All the experimental results imply that the selectivities of the MOFs are related to the structures and electronic properties of both the MOFs and the analytes as well as the nature of their interactions.

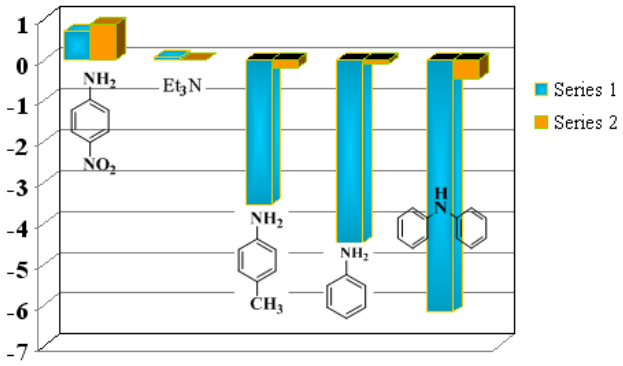

Fig. 4 Percentage of fluorescence quenching or enhancing of **1** obtained for different analytes in acetonitrile at room temperature.

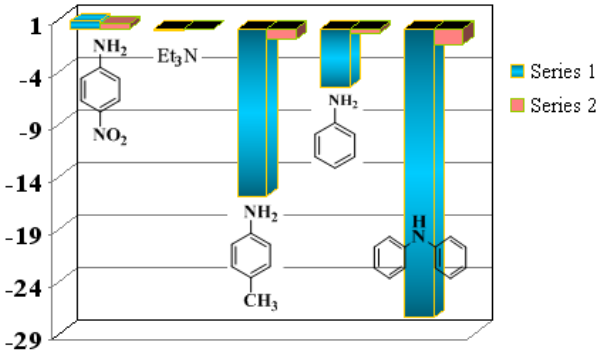

Fig. 5 Percentage of fluorescence quenching or enhancing of **2** obtained for different analytes in methanol at room temperature.

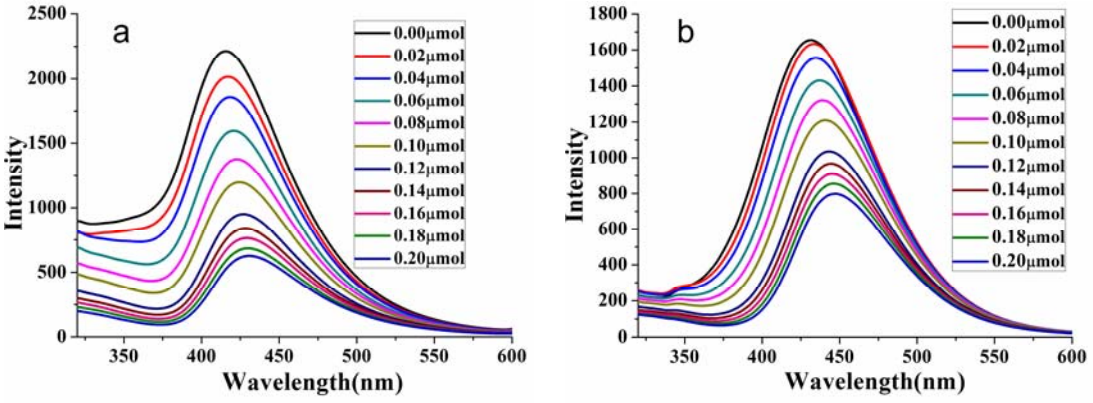

Fig. 6 Fluorescence titration of **1** (a) dispersed in acetonitrile and **2** (b) dispersed in methanol with the addition of different volume of 10^{-3} M acetonitrile or methanol solution of *p*-nitroaniline. The excitation wavelengths were both 310 nm and fluorescence emissions were monitored from 320 nm to 600 nm. The slit widths for both excitation and emission were 5 nm.

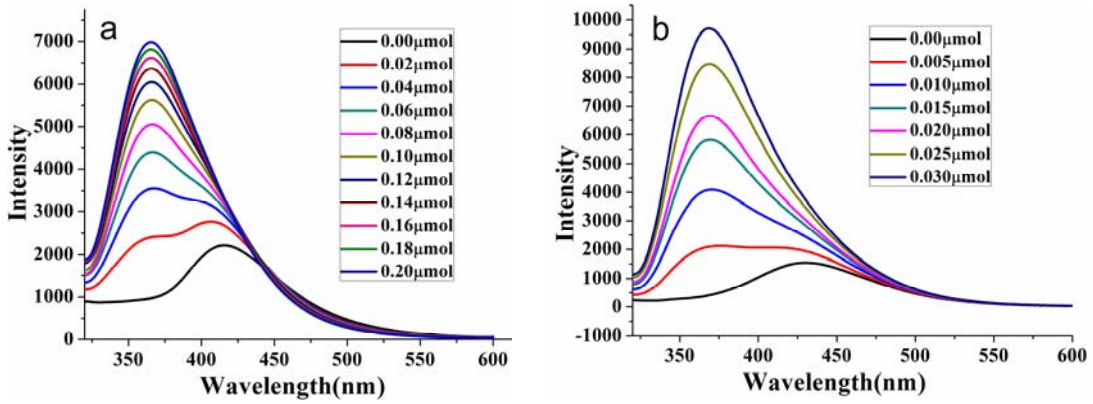

Fig.7 Fluorescence titration of **1** (a) dispersed in acetonitrile and **2** (b) dispersed in methanol with the addition of different volume of 10^{-3} M acetonitrile or methanol solution of diphenylamine. The excitation wavelengths were both 310 nm and fluorescence emissions were monitored from 320 nm to 600 nm. The slit widths for both excitation and emission were 5 nm.

3.4 Photocatalytic property study

Inspired by the photoresponses in the UV region of **1** and **2**, we have investigated the photocatalytic performances of **1** and **2** for the photodegradation of RhB under UV irradiation. As shown in Fig. S17 and S18, the absorption peaks of RhB have obviously decreased along with the prolonging of reaction time. The photocatalytic activities increase from 4.92% (without any catalyst) to 63.10% for **1**, 50.97% for **2** after 6 h under UV light irradiation. Their corresponding kinetics plots are shown in Fig. 8.

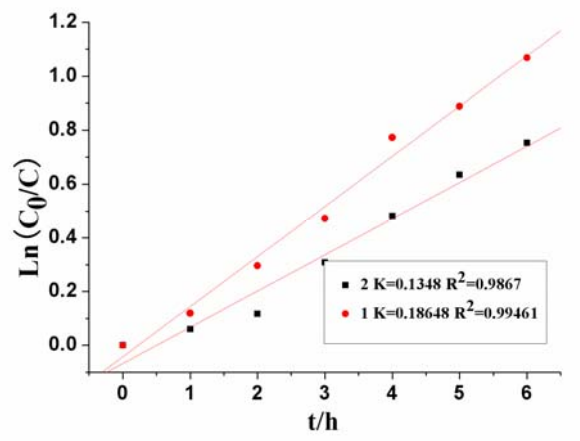

Fig. 8 The first-order plots for photodegradation of RhB of **1** and **2**

In addition, controlled experiments on the photodegradation of RhB have been carried out. Notably, no significant change in the degradation of RhB was observed in the following reaction conditions: (1) in the dark; (2) without catalyst; (3) under natural light (Fig. S19 − S23). These results demonstrate that the presence of both illumination and MOFs is necessary for the efficient degradation of RhB. Fig. 9 and Fig. 10 present the photocatalytic degradation profiles of RhB at different conditions, respectively. The increased degradation efficiencies compared with the controlled experiments indicate that both **1** and **2** are active for the decomposition of RhB in the presence of UV light irradiation. Moreover, the photocatalytic efficiency of **1** is higher than that of **2**. The difference in catalytic activity between them may be arising from the discrepancy in central metal ions of the two MOFs.

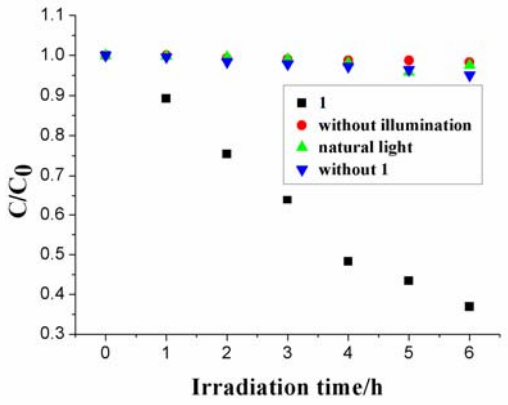

Fig. 9 The curves of degradation rate for RhB by **1** under different conditions

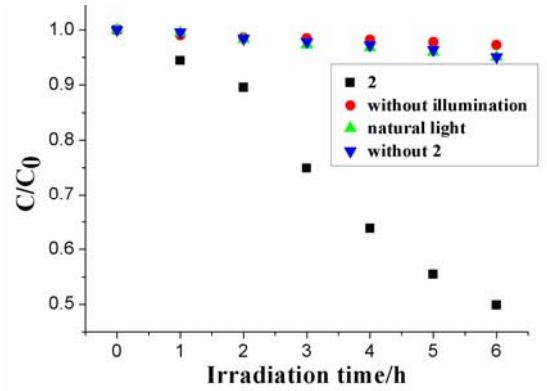

Fig. 10 The curves of degradation rate for RhB by **2** under different conditions

For the photocatalytic degradation reaction, the activity of the recycled catalyst is a very important factor for determining the performance of the photocatalyst. Herein, the photocatalytic reactions were re-examined five times under the irradiation of UV light. The results show that the recovered catalysts are nearly identical to the as-synthesized compounds. In addition, the photostabilities of the catalysts were monitored by using PXRD patterns and IR spectra during photocatalytic reactions. The PXRD patterns and IR spectra of MOFs had no notable differences before and after the photocatalytic cycles under UV light irradiation (Fig. S24 - S26). Also, the recycled MOFs exhibit similar photocatalytic performances with original MOFs (Fig. 11 and Fig. 12)**.** The results illustrate that **1** and **2** maintain their structural integrity after photocatalytic reactions. So, **1** and **2** may be good candidates for photocatalytic degradation of RhB.

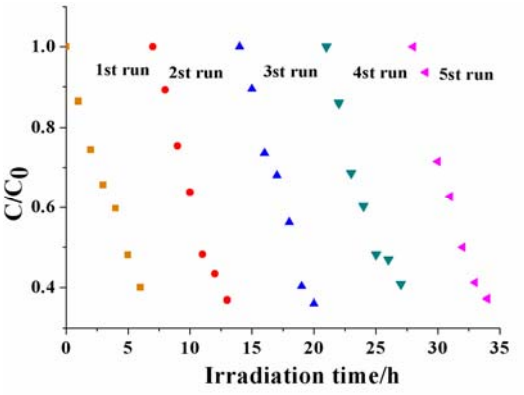

Fig. 11 Cycling runs of the photocatalytic degradation of RhB by **1** under UV light irradiation.

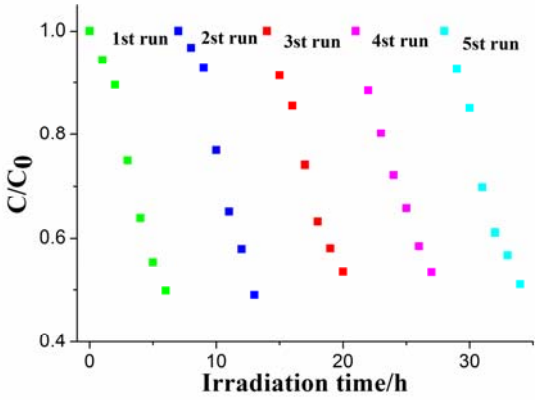

Fig. 12 Cycling runs of the photocatalytic degradation of RhB by **2** under UV light irradiation.

4. Conclusions

In summary, two luminescent transitional metal MOFs, $[ZnL\cdot H_2O]_n$ **(1)** and $[CdL\cdot H_2O]_n\cdot 2nH_2O$ **(2)** (L = 5-aminoisophthalic acid), were selected as candidates for selective sensing aromatic amines and degrading organic dyes. The fluorescence sensing experiments revealed that the two d^{10}-MOFs are highly sensitive towards aromatic amines but insensitive to aliphatic amine. For the selected aromatic amines, *p*-nitroaniline acts as an electron-deficient compound and greatly quenched the fluorescence intensities of the two MOFs. On the contrary, the other aromatic amines significantly enhanced the fluorescence intensities of the two MOFs. Moreover, the enhancing effect of diphenylamine is much larger than those of the others even at very low concentration, which is in accordance with the expectation based on the electron-rich of the analytes. These results confirm that the luminescent MOFs are promising fluorescence sensor materials for selectively detecting aromatic amines. Meanwhile, the excellent photocatalytic performances of both chemical stability and

readily regeneration make the MOFs good candidates for both heterogeneous photocatalyst and pollutants detectable materials.

Acknowledgements

This project is supported by NSFC (Grant no. 21271138), the NSF of Tianjin (No.14JCYBJC17500), the State Key Laboratory of Inorganic Synthesis and Preparative Chemistry of Jilin University (No. 2015-02) and The 2013 National College Students' innovation and entrepreneurship training program (201310058016).

Supplementary data

X-ray crystallographic file in CIF format (CCDC 1033338 for **1** and 1046705 for **2**). Crystal data (Table S1) and selected bond lengths and bond angles (Table S2). The hydrogen bonds data (Table S3). The TG curves and the PXRD patterns of **1** and **2** (Fig. S1−S4). The fluorescence spectra of **1** and **2** at the solid state and in different organic solvents (Fig. S5−S8). UV−vis diffuse-reflectance spectra of **1** and **2** (Fig. S9, S10). Fluorescence titration of **1** and **2** dispersed in acetonitrile or methanol with the addition of different analytes (Fig. S11−S16). UV/Vis absorption spectra of RhB solution degraded by **1** and **2** under different conditions (Fig. S17−S23). The PXRD patterns of **1** or **2** and recycled **1** or **2** (Fig. S24, S25). IR spectra of **1** or **2** before and after photocatalytic reactions. (Fig. S26).

References

[1] H. M. Pinheiro, E. Touraud, O. Thomas, *Dyes Pigments* 2004, **61**, 121–139.

[2] T. S. Scott, Elsevier, *Amsterdam*, 1962.

[3] L. M. Games, R. A. Hites, *Anal. Chem.* 1977, **49**, 1433–1440.

[4] J. L. Wang, G. D. Wang, G. A. S. Ansari, M. F. Khan, Toxicol. *Appl. Pharmacol* 2008, **230**, 227–234.

[5] J. Schubert, O. Kappenstein, A. Luch, T. G. Schulz, *J. Chromatogr. A* 2011, **1218**, 5628–5637.

[6] X. J. Huang, N. N. Qiu, D. X. Yuan, Q. M. Lin, *J. Chromatogr. A* 2009, **1216**

4354–4360.

[7] J. S. Chiang, S. D. Huang, *Talanta,* 2008, **75**, 70–75.

[8] X. J. Huang, T.Y. You, T. Li, X. R. Yang, E. K. Wang, *Electroanalysis* 1999, **11**, 969–972.

[9] A. Asthana, D. Bose, A. Durgbanshi, S. K. Sanghi, W. T. Kok, *J. Chromatogr. A* 2000, **895**, 197–203.

[10] N. Dossi, R. Toniolo, A. Pizzariello, S. Susmel, G. Bontempelli, *Electrophoresis* 2011, **32**, 906–912.

[11] X. E. Zhao, Y. R. Suo, *J. Sep. Sci.* 2008, **31**, 646–658.

[12] J. García-Lavandeira, C. Salgado-Petinal, E. Blanco, R. Cela, *Anal. Bioanal. Chem*. 2010, 397, 751–763.

[13] P. Sutthivaiyakit, S. Achatz, J. Lintelmann, T. Aungpradit, R. Chanwirat, S. Chumanee, A. Kettrup, *Anal. Bioanal. Chem*. 2005, **381**, 268–276.

[14] R. N. Li, L. L. Wang, X. T. Gao, G. F Dua, H. L. Zhai, X. Y Wang, G. S. Guo, Q. S. Pu, *Journal of Hazardous Materials* 2013, **248-249**, 268−275.

[15] H. K. Chae, D. Y. Siberio-Perez, J. Kim, Y. Go, M. Eddaoudi, A. J. Matzger, M. O'Keeffe, O. M. Yaghi, *Nature* 2004, **427**, 523–527.

[16] H. Furukawa, N. Ko, Y. B. Go, N. Aratani, S. B. Choi, E. Y. Choi, A. O. Yazaydin, R. Q. O'Snurr, M. Keeffe, J. Kim, O. M. Yaghi, *Science* 2010, **329** 424–428.

[17] N. L. Rosi, J. Eckert, M. Eddaoudi, D. T. Vodak, J. Kim, M. O'Keeffe, O. M. Yaghi, *Science* 2003, **300**, 1127–1129.

[18] B. Gole, A. K. Bar, P. S. Mukherjee, *Chem. Eur. J.* 2014, **20**, 2276–2291.

[19] S. Pramanik, C. Zheng, X. Zhang, T. J. Emge, J. Li, *J. Am. Chem. Soc.* 2011, **133**, 4153–4155.

[20] M. Myersa, A. Podolska, C. Heath, M. V. Baker, B. Pejcic, *Analytica Chimica Acta*. 2014, **819**, 78−81.

[21] S. B. Ding, W. Wang, L. G. Qiu, Y. P. Yuan, F. M. Peng, X. Jiang, A. J. Xie, Y. H. Shen, J. F. Zhu, *Materials Letters* 2011, **65**, 1385−1387.

[22] S. Achmann, G. Hagen, J. Kita, I. M. Malkowsky, C. Kiener, R. Moos, *Sensors*

2009, **9**, 1574−1589.

[23] Z. J. Zhang, S. C. Xiang, X. T. Rao, Q. A. Zheng, F. R. Fronczek, G. D. Qian, B. L. Chen, *Chem. Comm*. 2010, **46**, 7205−7207.

[24] S. S. Nagarkar, B. Joarder, A. K. Chaudhari, S. Mukherjee, S. K. Ghosh, *Angew. Chem*. 2013, **125**, 2953−2957.

[25] J. S. Qin, S. J. Bao, P. Li, W. Xie, D. Y. Du, L. Zhao, Y. Q. Lan, Z. M. Su, *Chem. Asian J.* 2014, **9**, 749−753.

[26] S. M. Hu, H. L. Niu, L. G. Qiu, Y. P. Yuan, X. Jiang, A. J. Xie, Y. H. Shen, J. F. Zhu, *Inorg. Chem. Comm*. 2012, **17**, 147−150.

[27] L. Q. Shi, C. He, D. F. Zhu, Q. G. He, Y. Li, Y. Chen, Y. X. Sun, Y. Y. Fu, D. Wen, H. M. Cao, J. G. Cheng, *J. Mater. Chem*. 2012, **22**, 11629−11635.

[28] P. Falcaro, F. Normandin, M. Takahashi, P. Scopece, H. Amenitsch, S. Costacurta, C. M. Doherty, J. S. Laird, M. D. H. Lay, F. Lisi, A. J. Hill, D. Buso, *Adv. Mater.* 2011, **23**, 3901–3906.

[29] D. X. Ma, B. Y. Li, X. Zhou, Q. Zhou, K. Liu, G. Zeng, G. H. Li, Z. Shi, S. H. Feng, *Chem. Commun.*, 2013, **49**, 8964–8966.

[30] L. L. Wen, L. Zhou, B. G. Zhang, X. G. Meng, H. Qua, D. F. Li, *J. Mater. Chem*. 2012, **22**, 22603−22609.

[31] W. Q. Kan, B. Liu, J. Yang, Y. Y. Liu, J. F. Ma, *Cryst. Growth & Des*. 2012, **12**, 2288−2298.

[32] C. Q. Xu, H. H. Wu, F. L. Gu, *Journal of Hazardous Materials* 2014, **275**, 185−192.

[33] R. Li, X. Q. Ren, H. W. Ma, X. Feng, Z. G. Lin, X. G. Li, C. W. Hu, B. Wang, *J. Mater. Chem. A*. 2014, **2**, 5724−5729.

[34] S. Q. Zhang, L. Han, L. N. Li, J. Cheng, D. Q. Yuan, J. H. Luo, Cr*yst. Growth & Des*. 2013, **13**, 5466−5472.

[35] C. D. Wu, C. Z. Lu, W. B. Yang, H. H. Zhuang, J. S. Huang, *Inorg. Chem.* 2002, **41**, 3302–3307.

[36] W. B Yuan, T. Liu, Z. G. Guo, H. F. Li, R. Cao, *J. Mol. Struc.* 2010, **965,** 82–88.

[37] Q. X. Liao, Y. G. Yao, *Chin. J. Struct. Chem.* 2006, 4, 465-468.

[38] K. L. Zhang, N. Qiao, H. Y. Gao, F. Zhou, M. Zhang, *Polyhedron* 2007, **26**, 2461-2469.

[39] J. Tao, X. Yin, Y. B. Jiang, R. B. Huang, L. S. Zheng, *Inorg. Chem. Commun*. 2003, **6**, 1171-1174.

[40] G. M. Sheldrick, SHELXS-97, P*rogram for Crystal Structure Solution, University of Göttingen*, *Germany* 1997.

[41] G. M. Sheldrick, SHELXL–97, *Program for Crystal Structure Refinement, University of Göttingen*, *Germany* 1997.

[42] G. M. Sheldrick, SADABS, P*rogram for Empirical Absorption Correction of the Area detector Data, University of Göttingen, Germany* 1996.

[43] S. Pramanik, Z. C. Hu, X. Zhang, C. Zheng, S. Kelly, J. Li, *Chem. Eur. J.* 2013, **19**, 15964−15971.

[44] J. M. Zhou, W. Shi, H. M. Li, H. Li, P. Cheng, J. *Phys. Chem. C*. 2014, **118**, 416−426.

[45] S. W. Thomas III, J. P. Amara, R. E. Bjork, T. M. Swager, *Chem. Commun*. 2005, **17**, 4572−4574.